Tone noise prediction of an open-fan engine using a source-mode integral formulation

Vincent Daydé-Thomas, Cyril Polacsek, Xavier Gloerfelt, Masakazu Sugiyama, Jacky Mardjono

forum acusticum 2023

TONE NOISE PREDICTION OF AN OPEN-FAN ENGINE USING A SOURCE-MODE INTEGRAL FORMULATION

Vincent Daydé-Thomas[1,2,3*] **Cyril Polacsek**[1] **Xavier Gloerfelt**[3]
Masakazu Sugiyama[1,2,3] **Jacky Mardjono**[2]
[1] DAAA, ONERA, Université Paris Saclay, F-92322 Châtillon, France
[2] Safran Aircraft Engines, Rond-point René Ravaud, Moissy-Cramayel, France
[3] DynFluid Laboratory, Arts et Métiers Institute of Technology, Paris, France

ABSTRACT

This study discusses the development of a tone noise model dedicated to an open fan engine, also called Unducted Single Fan. Because of its particular architecture, this engine aims to reduce fuel consumption, but it might increase the radiated noise due to the fairing removal. This model intents to be soon implemented into acoustic source mapping techniques to better characterize the dominant sources in future wind tunnel experiments. It is based on FW-H analogy relying on the thickness and loading noise terms of Goldstein's formulation, written in the frequency domain. A decomposition into angular modes through equivalent fixed phase-shifted sources is proposed. The predicted sound field takes in account different contributions, which are investigated here: the thickness noise, the steady and unsteady loading noise (from rotor and stator) in forward flight configurations, and including near-field effects. The unsteady loading harmonics are obtained from URANS calculations with eslA ONERA code. First predictions are compared to reference solutions provided by a time-domain FW-H solver, with fully non-compact sources involving a complete surface integration, at approach operating point. A more practical compact-source form is presented too.

Keywords: *Tone noise prediction, Source modes, Unducted Single Fan, Aeroacoustics*

***Corresponding author**: *vincent.dayde-thomas@safrangroup.com.*

1. INTRODUCTION

This work is undertaken in the framework of the development of greener aircraft engine architectures by Safran Aircraft Engines, and more specifically focused on the Unducted Single Fan (USF) configuration. Mainly designed for short to medium-range flights, this engine aims to reduce fuel consumption by increasing the by-pass ratio, and is characterised by its fairing-free propeller and stator. One main objective of this study is to assess the sound radiation from dominant harmonic sources over rotating blades and fixed vanes of generic USF architecture during wind-tunnel tests. Although well-known acoustic far-field formulations derived on FW-H analogy have been currently applied on propeller-driven aircraft [1], the USF architecture is novel and more challenging as different source mechanisms are involved. In particular, the flow interactions between the front propeller and the stator are expected to generate unsteady loadings on blades and vanes that could balance the steady loading noise contribution from isolated propeller. Moreover, the scattering effects in future installed configurations (only isolated configuration are investigated here), require the capture of acoustic near-field, usually neglected in far-field expressions. For that purpose, a fast Python tool is under development at ONERA with respect to previous requirements and aiming to be implemented in deconvolution-based source mapping techniques [2], for better identify the dominant sources in wind tunnel tests. The present formulation is derived from FW-H analogy starting from Goldstein's expressions [3] and then expressed in the frequency domain. In order to get a concise expression (more suitable for source localization implementation) a decomposition into angular modes and equivalent fixed phase-

shifted sources is proposed. The present model follows the principle of equivalent source distributions already applied in turbofans [4] and the so-called source-mode approach from Roger et al. [5]. It includes unsteady loadings on blades and vanes, in forward flight conditions (convection effects) and assumes, as a first step, zero angle of incidence. A first application of this source-mode model is discussed in this paper, with needed inputs (harmonic loadings) provided by URANS calculations performed with elsA ONERA code [6], more detailed in a complementary paper [7]. Approach operating conditions is considered and preliminary validations are addressed by comparing typical sound pressure level spectra and directivities with those obtained with a time-domain FW-H ONERA solver, KIM [8], with same CFD inputs. Compact-source formulations obtained by applying a suited integration of the blade/vane surface loadings along the chord and a distribution over radial strips are proposed too.
The studied configuration is briefly described in Sec. 2. Tone noise formulations are detailed in Sec. 3, with preliminary validations (for a point source) by comparison with usual far-field expressions. A brief overview of URANS calculations and post-processing that feed the model is done in Sec. 4. Then, Sec. 5 is devoted to acoustic predictions in terms of SPL spectra and directivities and first validations by comparisons with KIM solutions are discussed. Finally, preliminary conclusions and future work are addressed in Sec. 6.

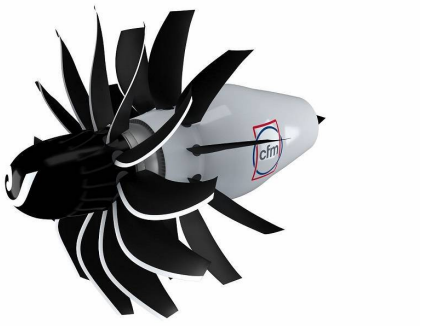

Figure 1. USF Engine demonstrator ©CFM

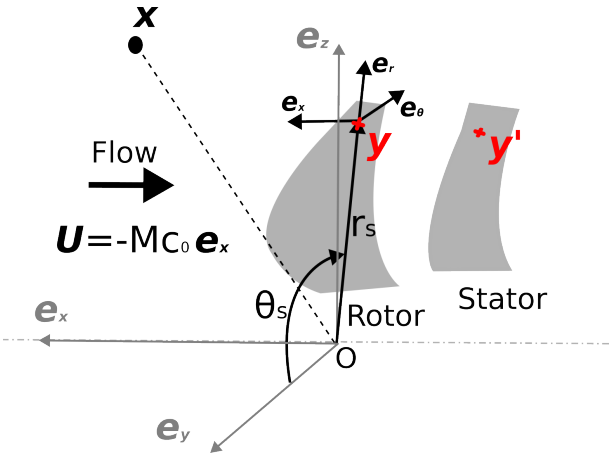

Figure 2. Main coordinate system

2. OPEN-FAN STUDIED CONFIGURATION

A generic USF architecture as considered in the present work is shown in Fig. 1. The studied Safran's R&T USF geometry has B-blades propeller and W-vanes stator, outlined in Fig. 2. We focus on approach operating point condition with propeller rotating speed around 600 RPM. As shown in Fig. 2, the propeller blades are strongly curved so that the radial contribution of the loadings (usually neglected) is questionable (see Sections 3 and 4). Due to the massive volume of air displaced by the highly tridimensional propeller blades, the contribution of the thickness component from the rotor is also analyzed. As the study takes place in the context of wind-tunnel experiments preparation, cylindrical coordinates are adopted in the mathematical description and for the analysis convenience. A general sketch of the reference frame and coordinate system is shown in Fig. 2.

3. TONE NOISE FORMULATIONS (PROPELLER AND STATOR

In this section, main equations derived from FW-H analogy are expressed in the coordinate system described in Fig. 2. The reference frame considered in the acoustic calculations is fixed and linked to the wind-tunnel. With this convention, the undisturbed fluid is in uniform translation $U_0 = M\,c_0$ in the direction $-\boldsymbol{e_x}$. We will consider a convected Green's function, G, solution of the convected wave equation associated to this frame, and so the convective derivative writing:

$$\frac{D}{Dt} = \frac{\partial}{\partial t} - U_0 \frac{\partial}{\partial x} \tag{1}$$

3.1 Tone noise formulations in frequency domain

Only the sources on propeller blades and the stator vanes are considered in this model, derived from FW-H solid

surface formulation. The engine is placed without incidence in an undisturbed fluid medium moving at a uniform Mach number M, while the observer is located at position coordinates $\boldsymbol{x}$ (x, y, z), with x pointing in the flight direction. The sources are located at coordinates $\boldsymbol{y}$ (x_s, y_s, z_s), with the prime symbol denoting the stator coordinates. Following Goldstein [3] and neglecting the quadrupole term, the starting equation can be written in the temporal domain as:

$$p(\boldsymbol{x}, t) = -\int_\tau \int_S \rho_0 V_n \frac{DG}{D\tau} dS(\boldsymbol{y}) d\tau + \int_\tau \int_S \boldsymbol{\nabla_y} G . \boldsymbol{F} dS(\boldsymbol{y}) d\tau \tag{2}$$

In Eqn. (2) V_n is the normal velocity of the fluid on the surface, ρ_0 the fluid density, $\boldsymbol{F}$ the loading projected on the surface: $F_i = p\, n_i$, and $\boldsymbol{\nabla_y} G$ the gradient of G related to the source coordinates. Let us consider the Green's function of a moving medium as expressed by Blokhintsev [9], written in the frequency domain as:

$$G_\omega = \frac{e^{-i\omega(\tau + \sigma/c_0)}}{4\pi T D} \tag{3}$$

τ being the emission time and c_0 the sound celerity, with T the period, D and σ the modified source-observer distances, and β the Lorentz factor:

$$\begin{aligned} D &= \sqrt{(x - x_s)^2 + \beta^2((y - y_s)^2 + (z - z_s)^2)} \\ \sigma &= \frac{M(x - x_s) + D}{\beta^2} \\ \beta &= \sqrt{1 - M^2} \end{aligned} \tag{4}$$

The Eqn. (2) can also be expressed in the frequency domain:

$$p(\boldsymbol{x}, \omega) = -\int_\tau \int_S \rho_0 V_n \frac{DG_\omega}{D\tau} dS(\boldsymbol{y}) d\tau + \int_\tau \int_S \boldsymbol{\nabla_y} G_\omega . \boldsymbol{F_s} dS(\boldsymbol{y}) d\tau \tag{5}$$

with $\boldsymbol{F_s}$ the loading harmonics. The sum of p_t and p_l, respectively thickness and loading terms can be written as:

$$p(\boldsymbol{x}, \omega) = p_t(\boldsymbol{x}, \omega) + p_l(\boldsymbol{x}, \omega) \tag{6}$$

3.2 Source-mode approach (non-compact source)

The noise emitted by a rotating source can be equivalently expressed as a continuous distribution of fixed phase-shifted sources placed circularly around the revolution axis. The phase shift is directly linked to the angular (spinning) mode order m, associated to the blade passing frequency (BPF), and trimmed by the well-known Tyler and Sofrin theory [10]:

$$m = nB - kW \tag{7}$$

The rotor-locked mode is given by $m = nB$, whereas interaction mode is expressed by Eqn. (7). This concept of "source-mode" [5] is also called "pulsing ring" [4] when using equivalent sources for turbofan applications. Starting with the thickness term which is monopolar, the strength of a monopole source located at the alpha position on the circle can be expressed as:

$$Q(\alpha, t) = Q(0, \frac{(nB)\alpha}{nB\Omega}) \tag{8}$$

The idea is to change variables in order to convert the time integral into an angular integral from 0 to 2π. The solution to the pulsing ring at the n-th BPF is expressed by putting $\theta_s = \Omega\tau$, with Ω the rotational speed. The convective derivative from Eqn. (1) is fully developed for the Green's function (Eqn. (3)). Denoting ω_{nB} the angular frequency corresponding to the BPF$_n$, the contribution of the B blades in the frequency domain yields to:

$$p_t(\boldsymbol{x}, \omega_{nB}) = \frac{\rho_0 B}{8\pi^2} \int_S \int_0^{2\pi} V_n [\frac{M c_0 (x - x_s)}{D^3} + i\frac{\omega_{nB}\sigma}{D^2}] e^{-i(k_{nB}\sigma + nB\theta_s)} d\theta_s dS \tag{9}$$

In the same way for the loading term, we can describe a dipolar point-source located at the α position on the circle by its strength that can be expressed, as shown in [5], by:

$$F(\alpha, t) = F(0, \frac{(nB - kW)\alpha}{nB\Omega}) \tag{10}$$

The gradient term of the Green's function from Eqn. (5) is expressed in cylindrical coordinates $\boldsymbol{y}$ (x_s, r_s, θ_s) as:

$$\boldsymbol{\nabla_y} G_\omega = \begin{pmatrix} \frac{\partial G_\omega}{\partial x_s} \\ \frac{\partial G_\omega}{\partial r_s} \\ \frac{1}{r_s}\frac{\partial G_\omega}{\partial \theta_s} \end{pmatrix} \tag{11}$$

After performing tedious algebra, the complete equation for the loading component can be formulated for homogeneous propeller and stator, with Eqn. (12) and Eqn. (13)

as:

$$p_l(\boldsymbol{x},\omega_{nB}) = \frac{B}{8\pi^2}\int_S \sum_{k=-\infty}^{+\infty} F_{s=kW}\int_0^{2\pi}\frac{n_i\zeta_i}{D}\cdot e^{-i(k_{nB}\sigma+(nB-s)\theta_s)}d\theta_s dS \quad (12)$$

$$p_l(\boldsymbol{x},\omega_{nB}) = \frac{W}{8\pi^2}\int_{S'} F_{s=nB}\sum_{k=-\infty}^{+\infty}\int_0^{2\pi}\frac{n'_i\zeta'_i}{D'}\cdot e^{-i(k_{nB}\sigma'+(s-kW)\theta'_s)}d\theta'_s dS' \quad (13)$$

with $n_i = (n_x, n_r, n_\theta)$ the outside normal components in cylindrical coordinates of the considered element, s denoting the loading harmonic order and ζ_i geometrical components defined as:

$$\zeta_i = \begin{pmatrix} \zeta_x = \frac{(x-x_s)}{D^2} + \frac{i\omega_{nB}}{c_0\beta^2}\left(\frac{x-x_s}{D}+M\right) \\ \zeta_r = K_r\left(\frac{1}{D}+\frac{i\omega_{nB}}{c_0\beta^2}\right) \\ \zeta_\theta = \frac{K_\theta}{r_s}\left(\frac{1}{D}+\frac{i\omega_{nB}}{c_0\beta^2}\right) \end{pmatrix} \quad (14)$$

With:

$$K_r = \frac{\beta^2(r\,cos(\theta-\theta_s)-r_s)}{D} \qquad K_\theta = \frac{\beta^2\, r_s\, r\, \sin(\theta-\theta_s)}{D} \quad (15)$$

and with the observer coordinates expressed in cylindrical coordinates too. It should be noted that the θ_s is a composition of multiple angles in the complete formulation: θ_{s0} which is the mode coordinates along the 0 to 2π integral, and ψ_c, ranging between ψ_{c1} and ψ_{c2} such as $\psi_c \in [\psi_{c1};\psi_{c2}]$, reflecting the angular range of the blade at a specific radius:

$$\theta_s = \theta_{s0} + \psi_c \quad (16)$$

For practical use, the pulsing ring is discretized and the integral over θ_s is replaced by a sum over N_q discrete position with the following equivalence:

$$\frac{1}{2\pi}\int_0^{2\pi} p_{nB,\theta_s}d\theta_s \approx \frac{1}{N_q}\sum_{j=1}^{N_q} p_{j,nB,\theta_s} \quad (17)$$

j denoting the indices of the discrete angular position of the source-mode. Furthermore, as proposed by Lévy [11], a radiation condition for the unsteady loading component in a convected medium can be simply written in the far-field as:

$$\frac{\Omega r_s}{c_0\beta} > \frac{|nB-kW|}{nB} \quad (18)$$

Indeed, in the near-field, evanescent spinning modes can still radiate and have an impact on the sound pressure level. In our application, Tab. 1 presents the radiated modes for the 3 first BPF, bold values referring to the rotor-locked modes (related to the steady loadings). According to the criterion of Eqn. (18) applied on our specific case, the number of spinning mode radiated in the far-field increases with the BPF order.

Table 1. Summary of loading harmonic orders with associated angular mode orders

BPF$_n$	Spinning mode order	Rotor loading harmonics order	Stator loading harmonics order
BPF1	**B**, $B-W$, $B-2W$	W, $2W$	B
BPF2	**2B**, $2B-W$, $2B-2W$, $2B-3W$ $2B-4W$	W,$2W$, $3W$, $4W$	$2B$
BPF3	**3B**, $3B-W$, $3B-2W$, $3B-3W$ $3B-4W$, $3B-5W$ $3B-6W$,	W, $2W$ $3W$, $4W$, $5W$, $6W$	$3B$

These above formulations have been implemented into an in-house Python code. An interface based on Zeppelin pre-processing tool (developed at ONERA by R.Barrier) provides the required inputs. The loading harmonics of order s are assessed from the time domain solution using a Fourier transform:

$$F_s = \frac{\Omega}{2\pi}\int_0^{2\pi/\Omega} F(t)e^{-is\Omega t}dt \quad (19)$$

where $F(t)$ is the unsteady pressure fluctuation over the blade/vane surface.

3.3 Validation by comparison with usual far-field expressions

Multiple far-field expressions for the tone noise can be found in the literature. First validation of the source-mode model is to compare its results with usual solutions from far-field formulations. For simplification purposes, this validation is performed on a single compact source point. The thickness contribution is assessed by considering the expression proposed by Lévy [11]. For the loading noise term, we refer to the expression derived by Hanson [1], with the radial component neglected. Both far-field formulations are relying on usual Bessel functions. Comparing each component with these formulation on a single

rotating source for the rotor simulating the thickness and the stationary loading, one shows the convergence in the far-field of the source-mode model in Fig. 3 and Fig. 4.

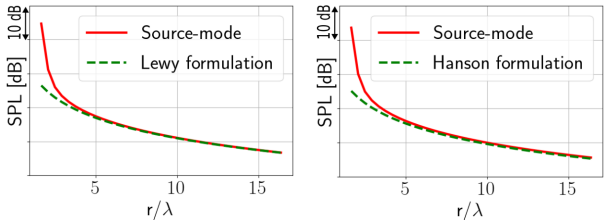

Figure 3. Far-field and source-mode SPL along r/λ for thickness (left) and stationary loading (right) for an observer in the rotor plane at BPF1

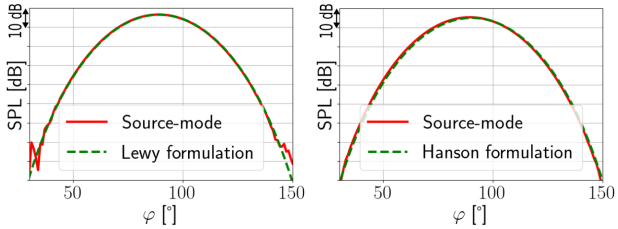

Figure 4. Comparison of the directivity at $r/\lambda = 19.2$ for BPF1 in the orthogonal plane to the rotor for thickness (left) and stationary loading (right)

In Fig. 4, φ is the polar angle in spherical coordinates at $r/\lambda = 19.2$ in the plan defined by x and z axis. As shown in Fig. 3, both solutions converge in the acoustic far-field for an expected value of r/λ around 3.5. Directivities are perfectly assessed by the model (Fig. 4), for the thickness component and the stationary loading component.

3.4 Source compacity along the chord

For source estimation purpose, it is desirable to reduce the number of unknowns (loading sources) to make it possible to resolve the inverse problem. For this reason, a compact formulation of the sources along the chord is proposed to simplify the surface integral into a lineic integral over the span (with compact sources at mean chord line center). This approach is sketched in Fig. 5. With these approximations, previous full non-compact formulations can be simplified to the following expressions for the rotor:

$$p_l(\boldsymbol{x}, \omega_{nB}) = \frac{B}{8\pi^2} \sum_{j=1}^{N_r} \sum_{k=-\infty}^{+\infty} \tilde{F}_{s=kW}(j\Delta r_s) \int_0^{2\pi} \frac{n_i.\zeta_i}{D_c} e^{-i(k_{nB}\sigma_c + (nB-s)\theta_s} d\theta_s \tag{20}$$

with:

$$\sigma_c = \frac{D_c + M(x - x_c)}{\beta^2} \qquad D_c = \sqrt{(x-x_c)^2 + \beta^2((y-y_c)^2 + (z-z_c)^2)} \tag{21}$$

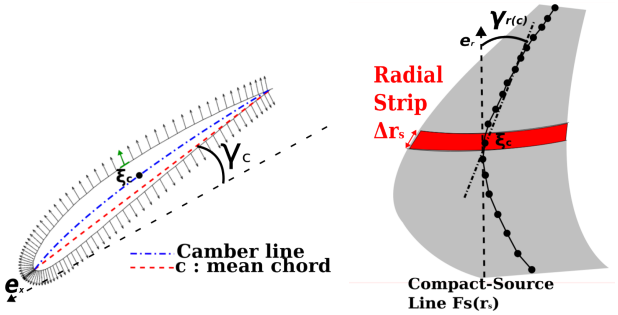

Figure 5. Integration into a compact source in chord

We can express in the same way the loading contribution of the stator as:

$$p_l(\boldsymbol{x}, \omega_{nB}) = \frac{W}{8\pi^2} \sum_{j=1}^{N'_r} \tilde{F}_{s=nB}(j\Delta r'_s) \sum_{k=-\infty}^{+\infty} \int_0^{2\pi} \frac{n'_i.\zeta'_i}{D'_c} e^{-i(k_{nB}\sigma'_c + (s-kW)\theta'_s} d\theta'_s \tag{22}$$

with the indices $_c$ denoting the compacted source point position, located here at mid-camber line.
Furthermore, because of the size of the engine and the relative position of the simulated antenna, non-compactness effects are expected to be significant, so that the inclusion of some non-compactness effects seems required. In this purpose, the phase shifts from the actual source points to the compact point (ξ_c) are taken into account in the chordwise integration of the loadings, meaning neglecting the distance discrepancies between respective source points

and observer.

$$\tilde{F}_s(\xi_c) = \int_{-c/2}^{c/2} F_s(\xi) n_\perp(\xi) e^{-ik_{nB}(\psi_\xi - \psi_c)} d\xi$$

$$\sigma_{\xi_c} = \frac{D_{\xi_c} + M(x_c - x_s)}{\beta^2}$$

$$D_{\xi_c} = \sqrt{(x_c - x_s)^2 + \beta^2((y_c - y_s)^2 + (z_c - z_s)^2)} \quad (23)$$

In this new description, $n_\perp$ denotes the outside normal to the mean chord line. In Eqn. (22), the normal components n_i are obtained for the two stagger angles of the equivalent profile (which is now assimilated to a flat surface): γ_r and γ_c (see Fig. 5). These ones are expressed as :

$$n_x = -\cos(\gamma_c); n_\theta = \sin(\gamma_c); n_r = \sin(\gamma_r) \quad (24)$$

4. INPUTS FROM URANS CALCULATIONS (OVERVIEW)

URANS CFD simulations were conducted using elsA ONERA solver [1] [6]. NASA's k-ω Wilcox [12] is used as turbulence model. The USF simulation domain is limited to a single channel using chorochronic approach, leading to a mesh of 25 million cells.
A complete description of these simulations are presented in [7]. As mentioned in Sec. 3, inputs to the Python code in terms of harmonic loadings and geometrical values (grid points, normals, surface elements) on blade/vane surfaces are directly provided using Zeppelin.

5. SOUND PREDICTIONS AND COMPARISONS WITH NUMERICAL SOLUTIONS

In this section, the model developed in Section 3.2 is compared to numerical solution obtained from ONERA's in-house code KIM.

5.1 Reference solution from time-domain FWH solver

The reference solution is obtained with the ONERA in-house code KIM [8]. This code includes several FW-H surface integral formulations with original formulas (including additional source terms for turbulent flows) and efficient processing for fairing-free rotating machinery applications. Calculations are performed in the time domain for structured or unstructured, fixed or moving, rigid or deformable meshes, including supersonic kinematics.

[1] Airbus-Safran-ONERA property

The code KIM is currently used for aeroacoustics studies by ONERA and its industrial partners.

5.2 Results with full surface integration

In order to reduce the computation time involved with the present model, the initial CFD mesh has been unrefined (non-regressive process checked but not shown for paper brevity), reducing the number of discrete elements by a factor of nearly 6. For code-to-code comparisons, observers are located on a common antenna: 26 microphones non-uniformly spaced in the x-direction (± 40 meters) located at $y = 0$ and $z = 15$ meters (with system coordinates of Fig. 2). The later named "Source-mode code" is a non-parallelized python code. Pre-processing, which contain mainly a refine module of the CFD mesh, is achieved using Cassiopée environment [13]. Complete time calculation, containing full surface integration, 10 BPF and all the contribution presented, is around 25 minutes on a desktop computer. For results using the compact sources model presented on section 3.4 (results not presented in this paper), computation time is around 40 seconds. For entire surface integration, directivities and spectra seen in this sections correspond to the approach operating point, with the rotor and stator contribution separated, and loading and thickness components also distinguished for the rotor.

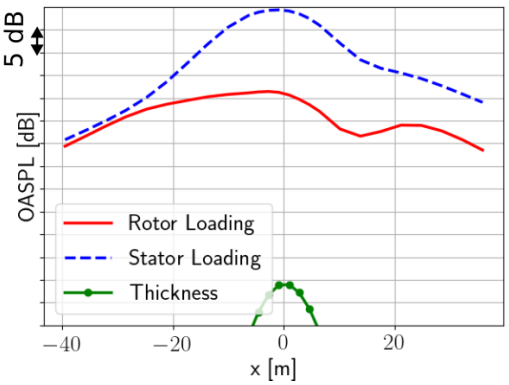

Figure 6. OASPL directivities

Firstly, we can observe on the OASPL directivity in Fig. 6 that the stator contribution is dominant. Wakes from the impacting the stator are the main contributors in the noise generation in this architecture at this specific operating point, corresponding to a low rotation speed. Further-

more, thickness component is far below loading component, and will not be longer take into account further in this paper. OASPL spectra obtained with KIM are rather similar. For accurate comparisons, we will focus on the SPL spectra obtained for the observer at $x = 0$, presented in Fig. 7 showing comparisons with reference solutions from KIM.

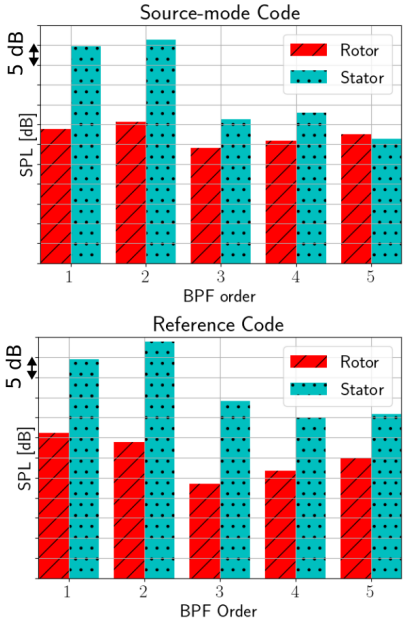

Figure 7. SPL spectrum for the source-mode and reference code (observer at $x = 0$ and $z = 15\,m$)

For each figure, the red lined bars represent the rotor contribution, and the blue pointed bars the stator contribution. A good agreement can be observed on first tones but more deviations are revealed at higher BPF. Focusing on the BPF1 and BPF2, we can take a closer look at their directivities in Fig. 8 and Fig. 9.

The source-mode code results are represented with a red straight line, and the KIM solver with a blue dotted line and labeled "Reference code". As shown in Fig. 8 and Fig. 9, the model captures very well the first harmonic, from extinctions to peaks, for rotor and stator cases. For BPF2, slight discrepancies can be observed, but the comparison is still satisfactory. Nevertheless, significant deviations have been pointed out from BPF3, without clear explanation (erroneous mode running is suspected). Investigations are underway to understand this mismatch from these preliminary results and to improve ongoing predictions.

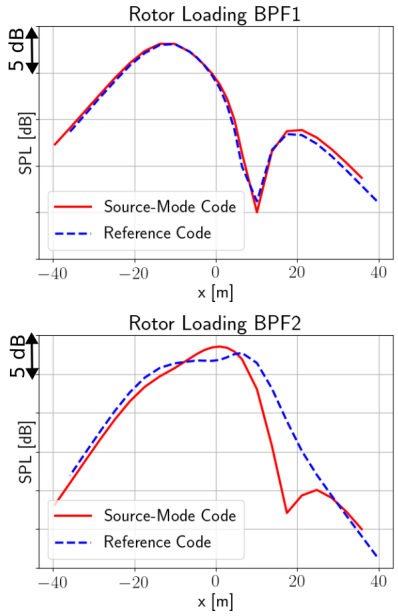

Figure 8. Directivity of the loading noise for the rotor BPF1 and BPF2

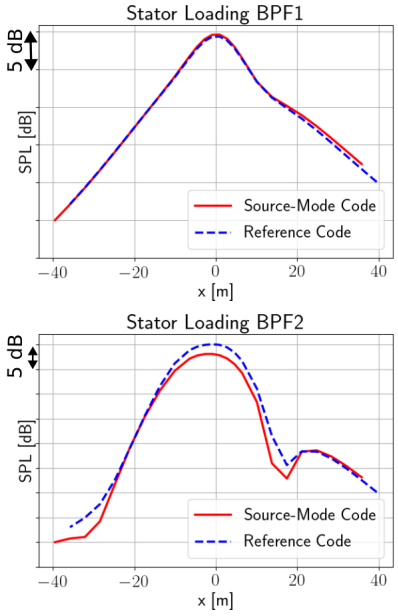

Figure 9. Directivity of the loading noise for the stator BPF1 and BPF2

6. CONCLUSION AND FUTURE WORK

This paper has presented a specific analytical model devoted to tone noise predictions applied a USF architecture and aiming to be implemented into ONERA's source mapping tools. A source-mode formulation based on FW-H analogy has been fully detailed and a simplified chordwise compact-source form, more suited to beamforming applications, has been described too. Basic validations with respect to usual far-field expressions from literature (involving Bessel functions) have been successfully addressed. Then, a first attempt of validation by comparison with reference solutions from an industrial FW-H solver (using common inputs provided by URANS calculations) has been discussed. Predictions performed at approach operating point have shown quite similar trends on OASPL spectra with a dominant contribution due to stator loadings. A good agreement has been shown on SPL directivities from propeller and stator at BPF1 and BPF2. However, significant deviations are observed on higher BPFs for which investigations are underway in order to explain this mismatch and to improve these results. Once present predictions are validated, next analysis will be focused on calculations using compact-source form.

7. ACKNOWLEDGEMENTS

This work was performed within the funding of Safran Aircraft Engines, through the funding of the Association Nationale de la Recherche Technologique (ANRT) and the French DGAC project MAMBO. This work was carried out with the technical support from ONERA.

8. REFERENCES

[1] D. B. Hanson, D. J. Parzych, and U. States., *Theory for noise of propellers in angular inflow with parametric studies and experimental verification*. National Aeronautics and Space Administration, Scientific and Technical Information Program ; National Technical Information Service, 1993.

[2] T. F. Brooks and W. M. Humphreys, "A deconvolution approach for the mapping of acoustic sources (DAMAS) determined from phased microphone arrays," *Journal of Sound and Vibration*, vol. 294, no. 4, pp. 856–879, 2006.

[3] M. Goldstein, *Aeroacoustics*. Advanced book program, McGraw-Hill International Book Company, 1976.

[4] C. Polacsek, G. Desquesnes, and G. Reboul, "An equivalent-source model for simulating noise generation in turbofan engines," *Journal of Sound and Vibration*, vol. 323, no. 3, pp. 697–717, 2009.

[5] M. Roger and K. Kucukcoskun, "Near-and-far field modeling of advanced tail-rotor noise using source-mode expansions," *Journal of Sound and Vibration*, vol. 453, pp. 328–354, 2019.

[6] L. Cambier, S. Heib, and S.Plot, "The Onera elsA CFD software: input from research and feedback from industry," *Mechanics & Industry*, vol. 14, no. 3, pp. 159–174, 2013.

[7] M. Sugiyama et al., "Noise prediction of an open fan using acoustic analogy approaches," in *Internoise 2023*, (Chiba, Japan), 2023 (in processing).

[8] J. Prieur and G. Rahier, "Comparison of Ffowcs Williams-Hawkings and Kirchhoff rotor noise calculations," 06 1998.

[9] D. Blokhintsev and U. S. N. A. C. for Aeronautics, *Acoustics of a Nonhomogeneous Moving Medium*. Technical memorandum (Translation of the Russian Original), National Advisory Committee for Aeronautics, 1956.

[10] J. M. Tyler and T. G. Sofrin, "Axial flow compressor noise studies," *SAE Transactions*, vol. 70, pp. 309–332, 1962.

[11] S. Lévy, "Prévision du bruit de raie émis par un rotor : application à l'aéronautique," *Journal de Physique IV Proceedings (French publication)*, vol. 04, no. C5, pp. C5–55–C5–65, 1994.

[12] D. C. Wilcox, "Formulation of the k-w turbulence model revisited," *AIAA Journal*, vol. 46, no. 11, pp. 2823–2838, 2008.

[13] C. Benoit, S. Péron, and S. Landier, "Cassiopee: A CFD pre- and post-processing tool," *Aerospace Science and Technology*, vol. 45, pp. 272–283, 2015.